Electronic Supplementary Information (ESI)

Supercapacitance in graphene oxide materials modified with tetrapyrrole dyes: A mechanistic study

Maciej Suchecki[a,b], Sylwia Klejna[a], Marianna Marciszko-Wiąckowska[a], Waldemar Bednarski[c], Natalia Rosiak[d], Kornelia Lewandowska[c], Konrad Szaciłowski[a]*

a. Academic Centre for Materials and Nanotechnology, AGH University of Science and Technology, al. A. Mickiewicza 30, 30-059 Kraków, Poland.

b. Faculty of Physics and Applied Computer Science, AGH University of Science and Technology, al. A. Mickiewicza 30, 30-059 Kraków, Poland.

c. Institute of Molecular Physics, Polish Academy of Sciences, ul. Smoluchowskiego 17, 60-179 Poznań, Poland.

d. Department of Pharmacognosy, Faculty of Pharmacy, Poznań University of Medical Sciences, Święcickiego 4, 60-781 Poznań, Poland.

E-mail: szacilow@agh.edu.pl

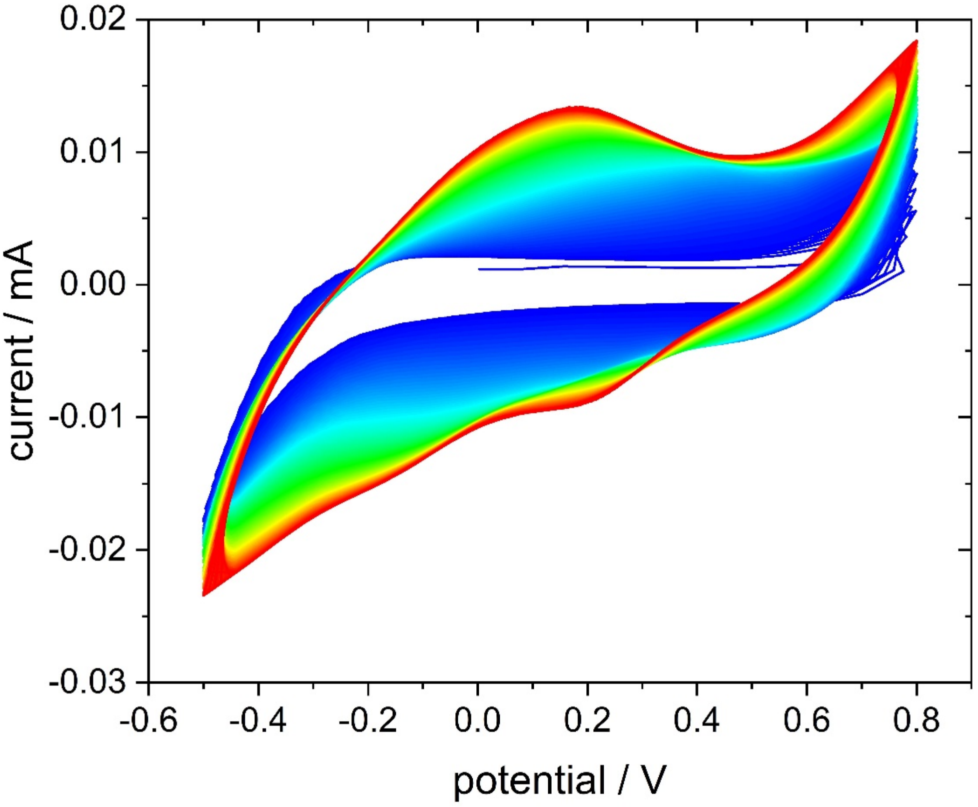

Figure S1. 700 voltamperograms recorded during 12 h of continuous cycling of the THPP@GO electrode in CsCl. Last 250 scans are identical, indicating the stabilization of the electrode.

Table S1 Selected characteristic absorption peaks of THPP, THPP@GO, TCPP and TCPP@GO and CuPC, and CuTAPC , CuPC@GO, and CuTAPC@GO. All values are given in nm.

	Soret bands		Q-bands	
	free dye	dye+GO	free dye	dye+GO
THPP	420	454		-
TCPP	424	444		-
CuPC	-	-	669	615, 700
CuTAPC	-	-	658, 681 600sh, 627 sh	669, 687 600sh

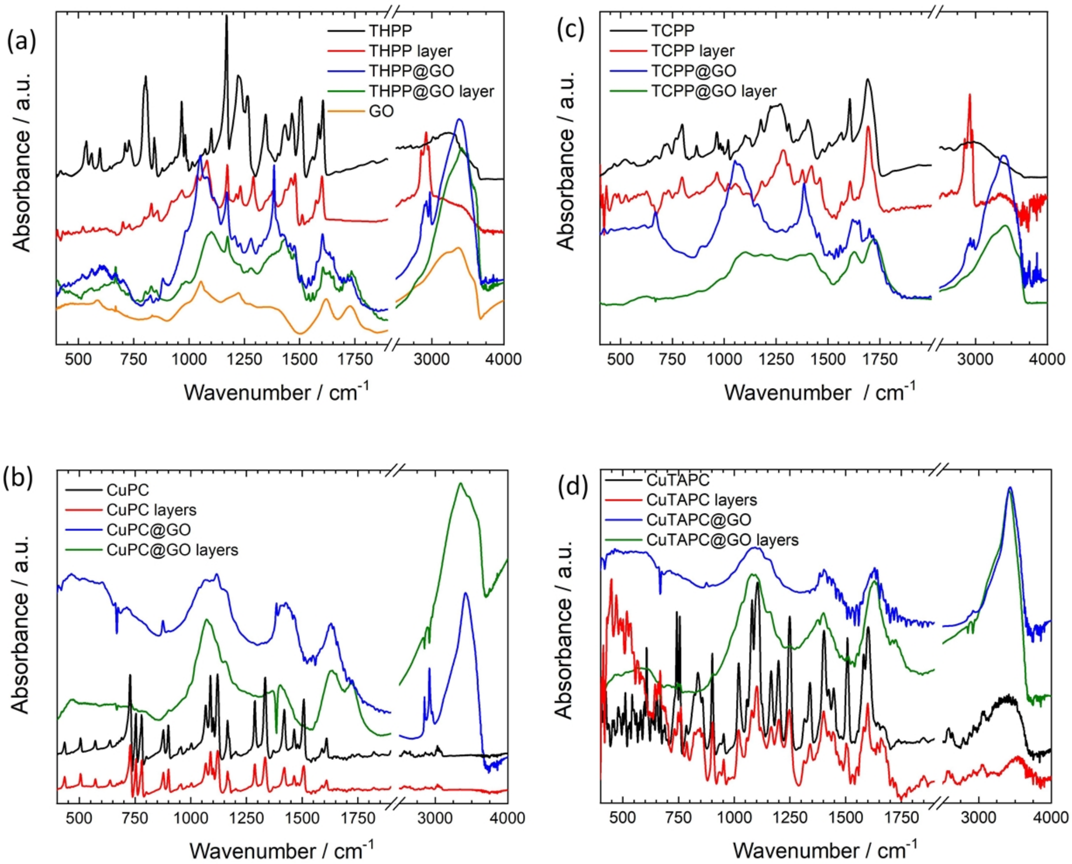

Figure. S2. Reflection–absorption spectra for 10 layers of thin films of THPP, THPP@GO (a), TCPP and TCPP@GO (b), CuPC, CuPC@GO (c) and CuTAPC, CuTAPC@GO (d) on Au (w) at the angle of incidence of 80 degrees (spectra in KBr are also displayed).

Table S2 Selected characteristic vibronic features of THPP, THPP@GO, TCPP and TCPP@GO and CuPC, and CuTAPC , CuPC@GO, and CuTAPC@GO. All energies are given in cm^{-1},(s-stretching, b-bending, w-wagging, r-rocking, def. deformation).

Sample	**IR KBr [cm^{-1}]**	**IR layers [cm^{-1}]**	**DFT [cm^{-1}]**	**Bands assignment**
THPP/ THPP@GO	535	536/**529**	542	C-H$_w$ in benzene + def. porphyrin ring
	560/**559**	566/**560**	568	C-H$_w$ in benzene + def. porphyrin ring
	597/**597**	599/ –	607	Breathing benzene + def. porphyrin ring
	729/-	729/**728**	764	N-H$_w$
	804/**803**	797/**803**	824	C-H$_w$ + N-H$_w$
	843/**852**	858/**853**	857	C-H$_w$ in benzene
	966/-	970/**967**	989	C-C$_s$ (breathing of pyrolle rings)
	983/**984**	985/**989**	1008	C-C$_s$ (breathing of pyrolle rings)
	-/1052			C-O s in GO
	1100/**1082, 1115**	1080/**1100**	1128	C-H$_r$ in benzene
	1169/**1170**	1175/**1171**	1197	C-O-H$_b$ in aryl substituents + C-H$_r$ in benzene
	1223/**1208**	1213/-	1199	C-O-C$_b$ in aryl substituents + C-H$_r$ in benzene
	1263/**1230**	1232/**1234**	1308	C-O$_s$ + C-H$_r$
	1346/**1385**	1373/**1387**	1370	C-H $_r$ + C-O-H $_b$
	1402/-	-/-	1439	C-H$_r$ in porphyrin + C-C$_s$ in porphyrin
	1433/**1458**	1461/**1455**	1466	C-H$_r$ in benzene + C-O-H$_b$
	1465/**1474**	1480/**1475**	1515	C=C$_s$ in methine and pyrolle rings
	1508/**1508**	1512/**1506**	1555	C-C$_s$ in benzene + C-H$_r$ + C-C$_s$ bond between porphyrin and aryl substituents
	1556/**1558**	1558/**1558**		C=C $_s$ + C-N-H $_b$
	1586/**1579**	1575/**1579**	1635	C-C$_s$ in benzene + C-O-H$_b$ bond
	1605/**1603**	1600/**1604**	1668	C-C$_s$ + C=C$_s$ in benzene and aryl substituents
	-/1726	**-/1736**		C=O s in GO
TCPP/ TCPP@GO	723/-	732/ –	763	N-H$_w$
	797/**796**	798/-	824	N-H$_w$ + C-H$_w$ in porphyrin
	866/**893**	866/**874**	884	C-H$_w$ + def. pyrolle rings
	964/-	965/-	989	Breathing pyrolle and benzene rings
	980/**983**	-/**983**	1008	Breathing pyrolle rings
	994/-	994/-	1022	C-N$_s$ + C-H$_r$ in porphyrin + N-H$_r$
	1019/**1019**	1018/-	1039	C-H$_r$ in benzene + N-H$_r$
	-/1050			C-O s in GO
	1101/**1091**	1121/1100	1118	C-O$_s$ + C-H$_r$
	1176/**1163**	1181/**1179**	1195	C-H$_r$ + C-O-H$_b$
	1221/**1230**	1225/**1224**	1220	C-H$_r$ + C-O-H$_b$ + N-H$_r$ + C-N$_s$
	1270/**1277**	1284/**1277**	1391	C-O-H$_b$ + C-C$_s$ in aryl substituents + C-N$_s$ + C-C$_s$ in porphyrin + C-H$_r$
	1310/**1317**	1314/**1319**	1417	C-C$_s$ + C-N$_s$ + C-H$_r$ in porphyrin
	1384/**1384**	1377/**1370**	1441	C-N $_s$ + C-C$_s$ + C=C$_s$ + C-Hr in porphyrin
	1473/**1471**		1518	C=C$_s$ in methine and pyrolle rings

	1505/**1512**	1509/-		C=C$_{s}$ + C-C$_{s}$ + C-H$_{r}$ + N-H$_{r}$
	1564/**1558**	1568/ –	1614	C=C$_{s}$ in pyrolle rings
	1605/**1616**	1605/**1625**	1660	C=C$_{s}$ + C-C$_{s}$ in benzene
	1691/**1698**	1693/**1699**	1818	C=O$_{s}$ in aryl substituents and GO
	-/**1724**	-/**1720**		C=O s in GO
CuPC/CuPC@GO	634/-	637/-		C-C oop
	729/**727**	729/**730**		C-H oop + C-N b in isoindole
	754/**754**	753/-		C-H oop
	780/**783**	781/-		C-N s + C-H oop + Cu-N s
	797/**801**	800/-		C-C oop + C-H oop
	875/**874**	876/		C-H oop + def all molecule
	900/**900**	900/**901**		Metal ligand vibration + C-N=C b + C-C-C b
	954/**957**	956/**965**		C-N=C b + C-H oop
	983/**991**	984/**995**		C-H oop
	1002/**1034**	1003/**1022**		C-H r + breathing isoindole
	1067/**1066**	1066/**1071**		C-C s + C-N s + Cu-N s + C-H r
	1090/**1094**	1090/**1091**		C-H r + C-N s + Cu-N b
	1120/**1117**	1122/**1122**		C-H r + breathing isoindole
	1166/**1161**	1165/**1155**		C-N s + C-H r
	1202/**1204**	1201/**1200**		C-C s $_{+}$ C-N s + C-H r
	1289/**1283**	1285/**1290**		C-N s in isoindole + C-H r
	1334/**1334**	1333/**1334**		C-C s in isoindole + C-N s
	1371/-	1369/**1366**		C-N s + C-C s
	1418/**1409**	1420/**1400**		C-C s in isoindole + C-H r
	1463/**1461**	1464/-		C-H r
	1480/-	1480/-		C-N s + C=N s + C-C s + C-H r
	1508/**1512**	1504/**1507**		C=N s
	1587/**1585**	1588/-		C=C s
	1609/**1626**	1607/**1629**		C=C s
		-/**1717**		C=O in GO
CuTAPC/CuTAPC@GO	742/748	748/**747**		C-C oop + C-N oop + C-N=C b + Cu-N s + def. isoindole
	784/-	788/-		C-N s
	832/-	837/-		Breathing isoindole + C-C s + Cu-N s + C-H oop
	901/906	902/**902**		Metal ligand vibration + C-N=C b + C-C-C b + C-C s
	1019/-	1019/**1029**		C-H r + C-N s
	1080/1078	1079/**1079**		C-C s + C-N s + C-H r
	1103/1091	1100/**1093**		C-N s + C-H r + Cu-N b
	1165/1155	1165/**1157**		C-N s + C-H r in isoindole
	1197/1199	1198/**1202**		C-H r + C-C s in isoindole
	1248/1246	1247/**1248**		C-N s + C=N s + C-C s in isoindole
	1339/1330	1340/-		C-C s + C-N s in isoindole + Cu-N s
	1403/1403	1400/**1397**		C-H r
	1447/1443	1443/**1443**		C-N s + C-C s + C-H r
	1507/1513	1503/**1511**		C=N s
	1580/1586	1581/-		C=C s
	1600/1610	1599/**1625**		C=C s

		-/**1720**		C=O s in GO

Table S3. The orientation of porphyrin rings (in films) of the selected complex with GO determined from IRRA spectra; the references are from bulk spectra of the adequate complex.

Sample	**C-O**		**C-N**		**C=C**		**C=C**		**C=O**	
	cm^{-1}	**θ [°]**	**cm^{-1}**	**θ [°]**	**cm^{-1}**	**θ [°]**	**cm^{-1}**	**θ [°]**	**cm^{-1}**	**θ [°]**
THPP	1232	38	1381	34	1480	37	1600	39		
THPP@GO	1234	42	1387	40	1475	43	1604	46		
TCPP	1314	40	1377	38			1605	50	1693	41
TCPP@GO	1319	43	1370	39			1625	42	1699	48
	C-C				**C=N**					
CuPC	1201	42	1369	45	1504	40	1607	46		
CuPC@GO	1200	45	1366	50	1507	43	1626	51		
CuTAPC	1079	44	1247	43	1503	42	1599	44		
CuTAPC@GO	1079	45	1248	48	1511	45	1625	49		

Table S4 Structural analysis of phthalocyanines and porphyrins GO complexes formed through hydrogen bonding; d [Å] – length of the bridging hydrogen bond between modifier and GO.

THPP@GO	**d [Å]**	**TCPP@GO**	**d [Å]**	**CuTAPC@GO**	**d [Å]**	**CuPC@GO**	**d [Å]**
OH^{THPP} – OH^{GO}	2.00	O^{TCPP} – HO^{GO}	1.78	N^{CuTAPC} – HO^{GO}	1.93	H^{CuPC} – OH^{GO}	3.06
OH^{THPP} – O^{GO}	1.79	OH^{TCPP} – O^{GO}	1.86	N^{CuTAPC} – HO^{GO}	1.86	H^{CuPC} – OH^{GO}	2.66
OH^{THPP} – OH^{GO}	2.01	O^{TCPP} – HO^{GO}	1.80	N^{CuTAPC} – HO^{GO}	1.98	H^{CuPC} – OH^{GO}	3.07
OH^{THPP} – O^{GO}	1.79	OH^{TCPP} – O^{GO}	1.82	N^{CuTAPC} – HO^{GO}	1.87	H^{CuPC} – OH^{GO}	2.70

Table S5 Structural, energetic and charge transfer analysis of porphyrin and GO complexes formed through different variants of hydrogen bonding.

	E_{ads} [eV]	**Q_{Bader} [*e*]**
THPP@GO		
$-OH^{THPP} \rightarrow -OH^{GO}$	-2.69	-0.287
$-OH^{THPP} \rightarrow =O^{GO}$	-2.60	-0.451
TCPP@GO		
$-OH^{TCPP} \leftarrow -OH^{GO}$	-2.61	+0.030
$-OH^{TCPP} \rightarrow =O^{GO}$	-2.24	-0.015
$=O^{TCPP} \rightarrow -OH^{GO}$	-2.78	-0.087

The negative value of Bader charges (Q_{Bader}) corresponds to the electron charge transfer from modifier to GO, positive – from GO to modifier; direction of the arrow marks the direction of the charge transfer.

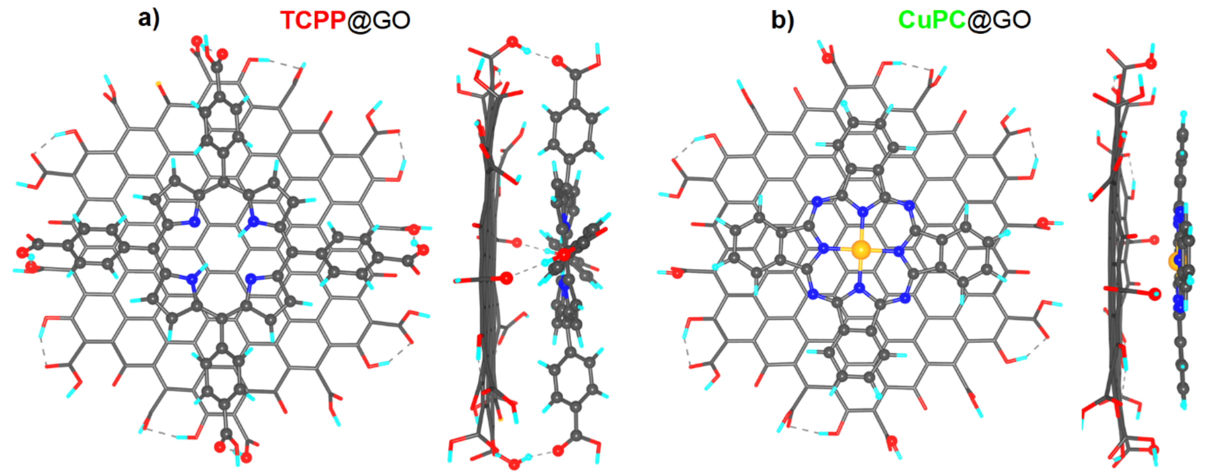

Figure S3. Top and side view of the atomic structure of hydrogen bond complexes a) TCPP@GO, b) CuPC@GO. Colour code: C in dark grey, N in blue, H in cyan, O in red, Cu in orange. Optimized with PAW-PBE-D3 method.

Table S6 Energetic and structural properties of phthalocyanines and porphyrins GO complexes; charge density analysis.

	E_{ads} [eV]	**d_{eq} [Å]**	**Q_{Bader} [e]**	**$\mu(z)$ [D]**	**$\Delta V(z)$ [eV]**
THPP@GO	-2.93	3.9 $d_{NH**NH–C\text{-}ring}$	-0.419	-5.13	+1.07
TCPP@GO	-3.39	3.8 $d_{NH**NH–C\text{-}ring}$	+0.009	-0.31	+0.07
CuTAPC@GO	-3.22	3.6 $d_{Cu–C\text{-}ring}$	-0.128	-2.12	+0.45
CuPC@GO	-3.35	3.5 $d_{Cu–C\text{-}ring}$	-0.037	-0.85	+0.18

Adsorption energies (E_{ads}) and equivalent distance (d_{eq}) computed with PAW-PBE-D3 for GO flake modified with THPP, TCPP, CuTAPC, CuPC.

Charge density analysis of complexes: Bader charges (Q_{Bader}) – negative value corresponds to the electron charge transfer from modifier to GO, positive – from GO to modifier; interface dipole moment ($\mu(z)$); interface electrostatic potential energy ($\Delta V(z)$).

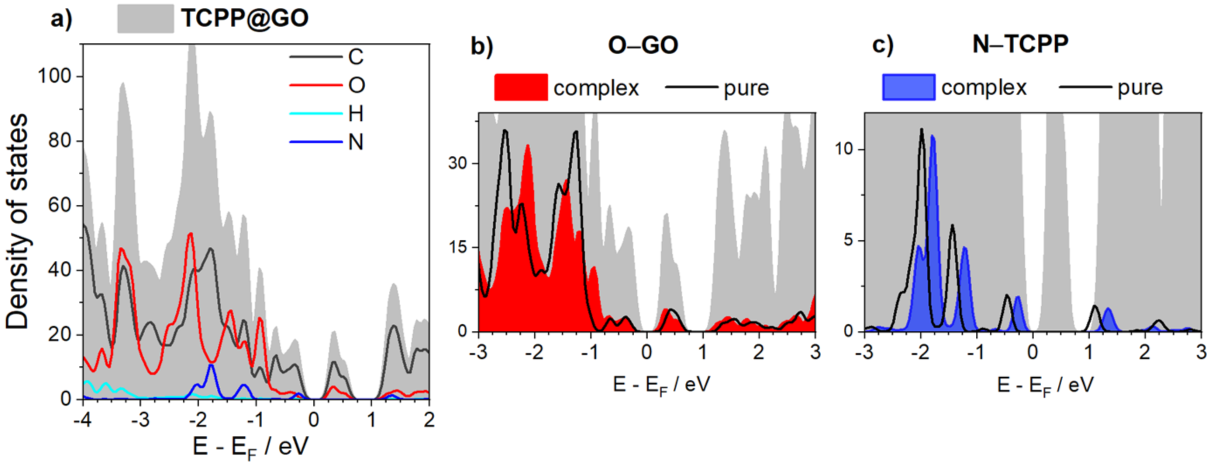

Figure S4. The density of states analysis for TCPP@GO complex: a) total and atom-projected DOS of TCPP@GO; b) oxygen-projected DOS of GO in the complex and pure GO; c) nitrogen-projected DOS of TCPP in the complex and pure TCPP.

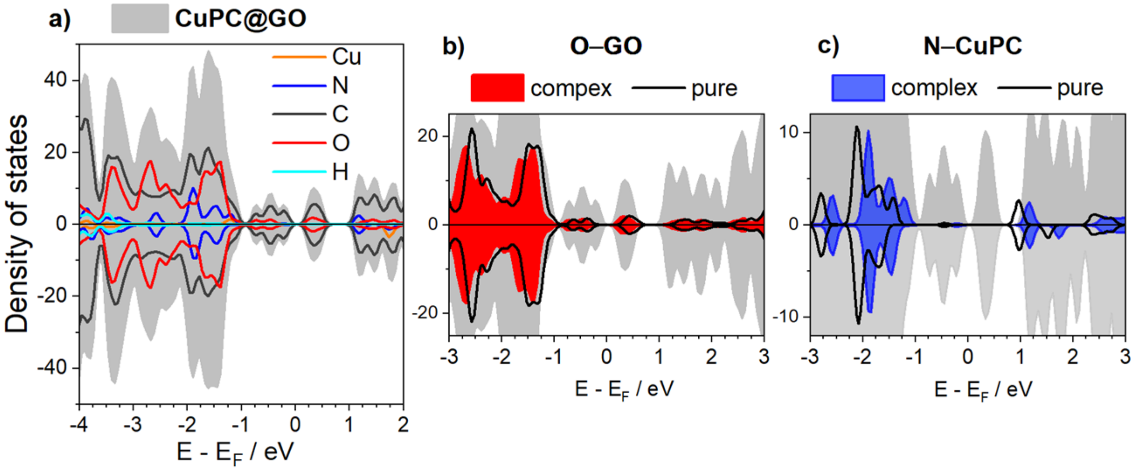

Figure S5. The density of states analysis for CuPC@GO complex: a) total and atom-projected DOS of CuPC@GO; b) oxygen-projected DOS of GO in the complex and in pure GO; c) nitrogen-projected DOS of CuPC in the complex and pure CuPC.

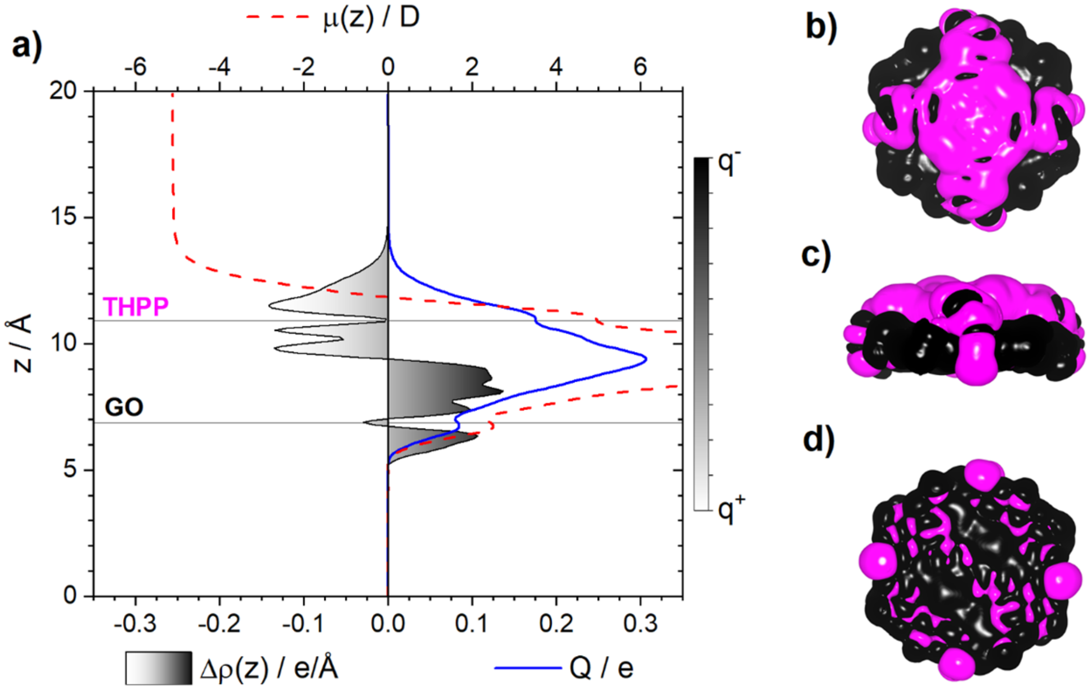

Figure S6. Details of the charge density difference analysis for THPP@GO complex: a) $\Delta\rho(z)$ – planar-averaged charge density difference, Q – integrated charge, $\mu(z)$ – interface dipole moment; black (white) corresponds to electron charge accumulation, q- (depletion, q^+); b) top (THPP exposure), c) side and d) bottom (GO exposure) view on isosurfaces of electron charge density difference; black (magenta) corresponds to electron charge accumulation, q- (depletion, q+).

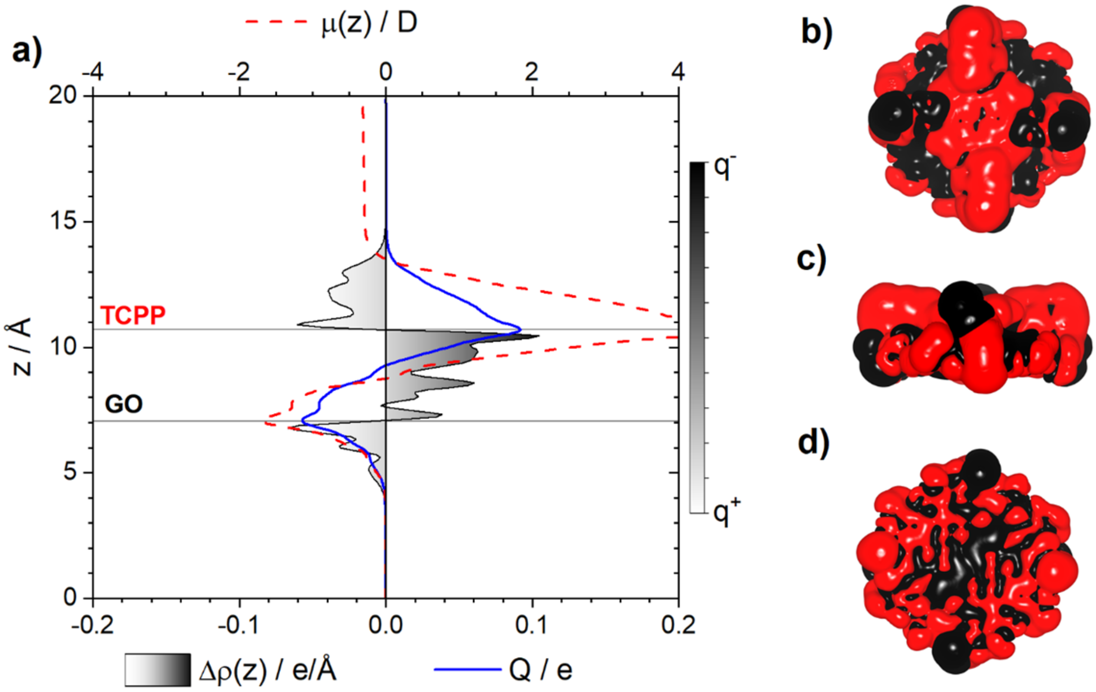

Figure S7. Details of the charge density difference analysis for TCPP@GO complex: a)$\Delta\rho(z)$ – planar-averaged charge density difference, Q – integrated charge, $\mu(z)$ – interface dipole moment; black (white) corresponds to electron charge accumulation, q- (depletion, q^+); b) top (TCPP exposure), c) side and d) bottom (GO exposure) view on isosurfaces of electron charge density difference; black (red) corresponds to electron charge accumulation, q- (depletion, q+).

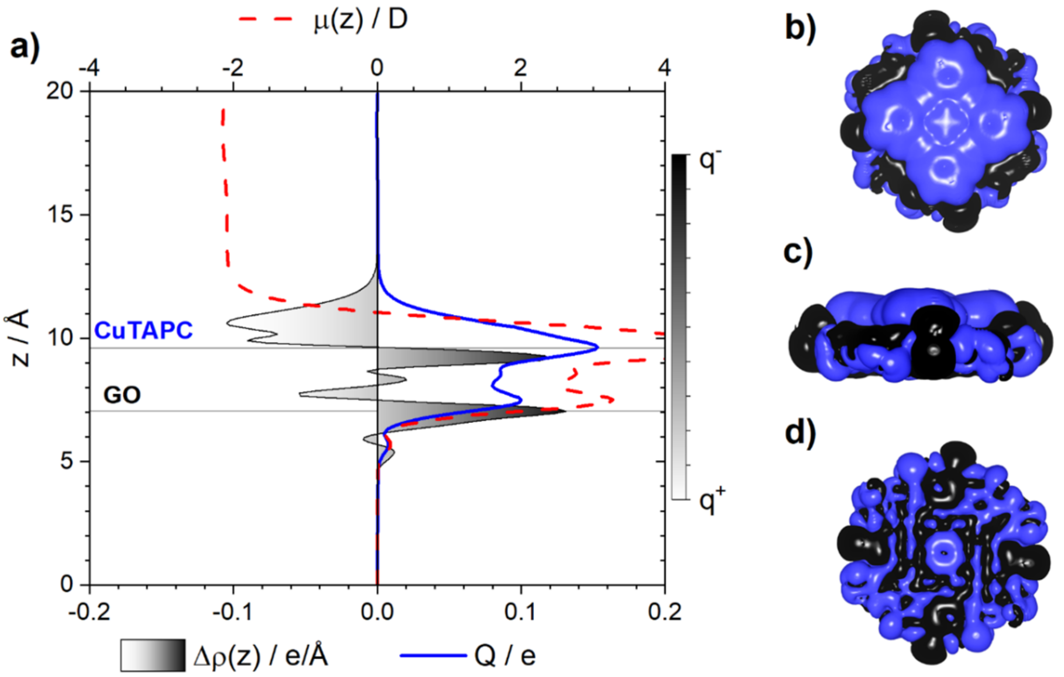

Figure S8. Details of the charge density difference analysis for Cu-TAPC@GO complex: a)$\Delta\rho(z)$ – planar-averaged charge density difference, Q – integrated charge, $\mu(z)$ – interface dipole moment; black (white) corresponds to electron charge accumulation, q- (depletion, q^+); b) top (CuTAPC exposure), c) side and d) bottom (GO exposure) view on isosurfaces of electron charge density difference; black (yellow) corresponds to electron charge accumulation, q- (depletion, q+).

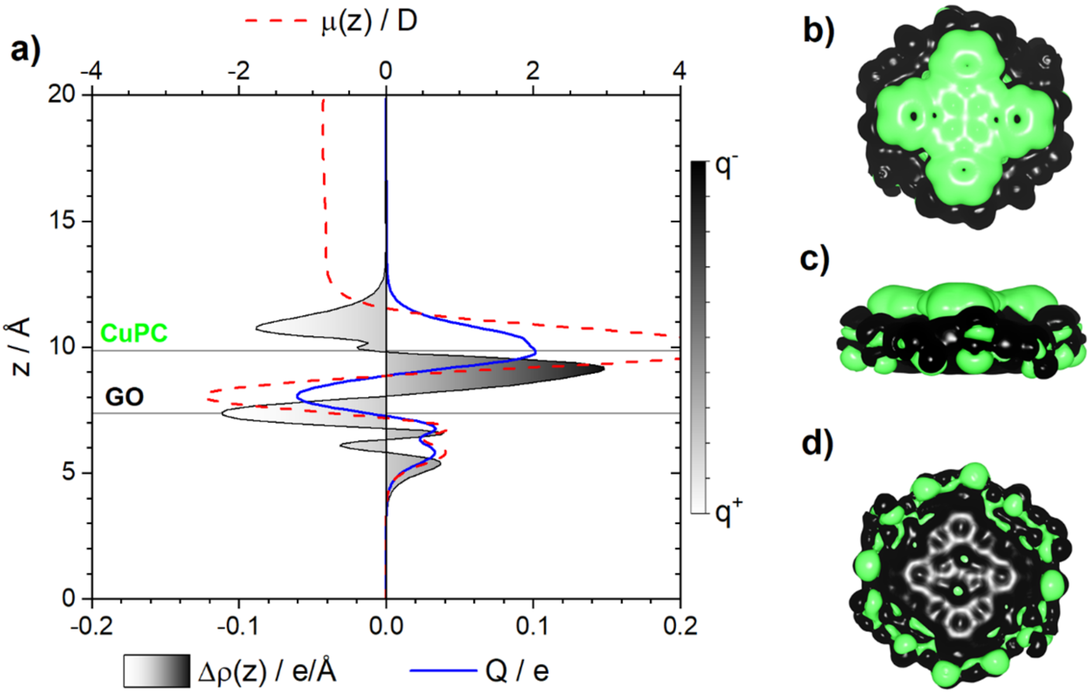

Figure S9. Details of the charge density difference analysis for CuPC@GO complex: a)$\Delta\rho(z)$ – planar-averaged charge density difference, Q – integrated charge, $\mu(z)$ – interface dipole moment; black (white) corresponds to electron charge accumulation, q- (depletion, q^+); b) top (CuPC exposure), c) side and d) bottom (GO exposure) view on isosurfaces of electron charge density difference; black (green) corresponds to electron charge accumulation, q- (depletion, q+).

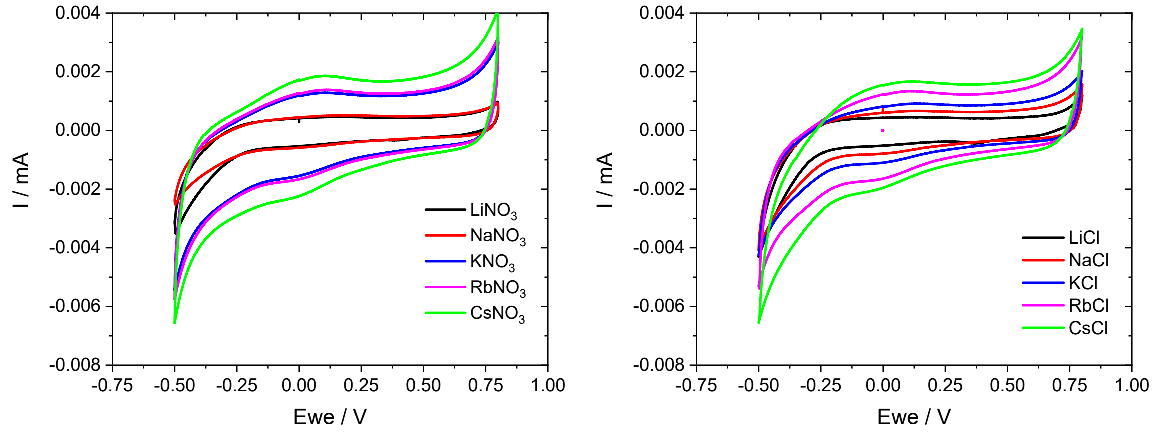

Figure S10. CV sweeps in a range from -0,8 V to 0,5 V for CuPC@GO in nitrates electrolytes (left) and chlorides (right).

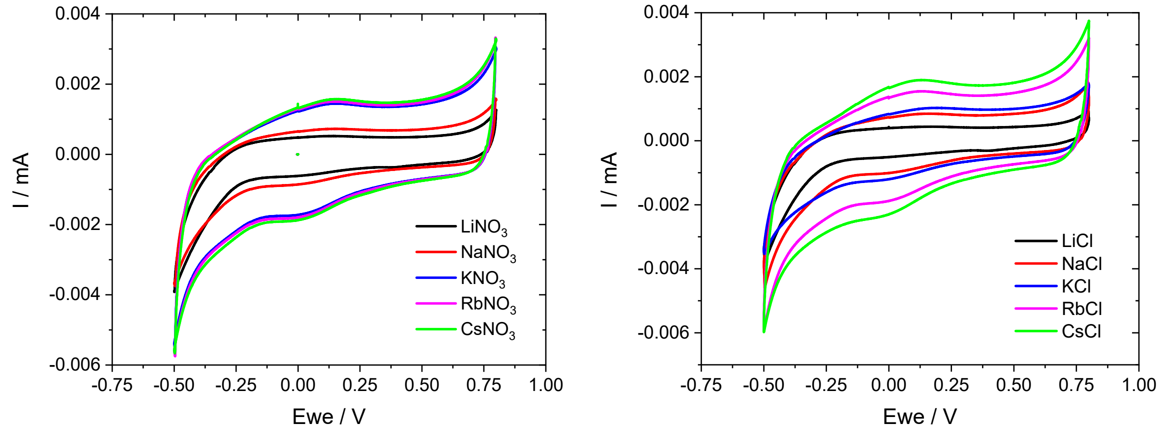

Figure S11. CV sweeps in a range from -0,8 V to 0,5 V for TCPP@GO in nitrates electrolytes (left) and chlorides (right).

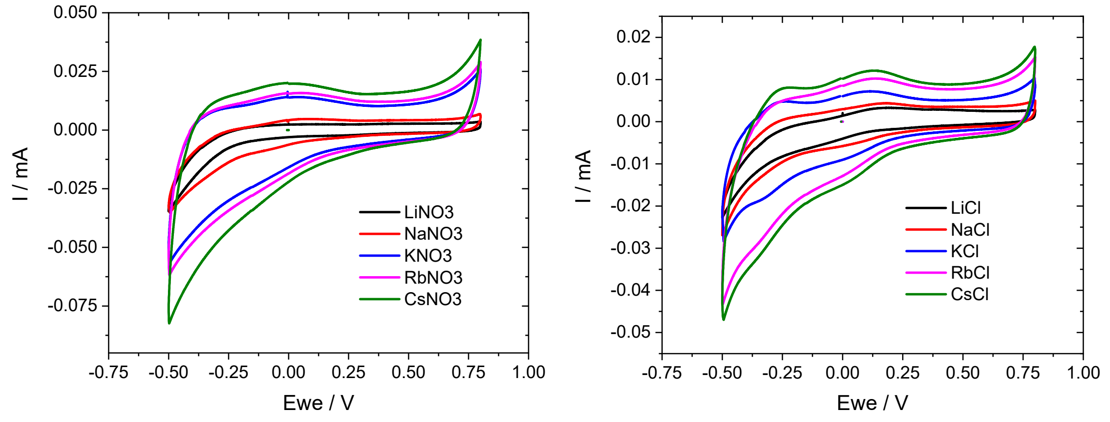

Figure S12. CV sweeps in a range from -0,8 V to 0,5 V for CuTAPC@GO in nitrates electrolytes (left) and chlorides (right).

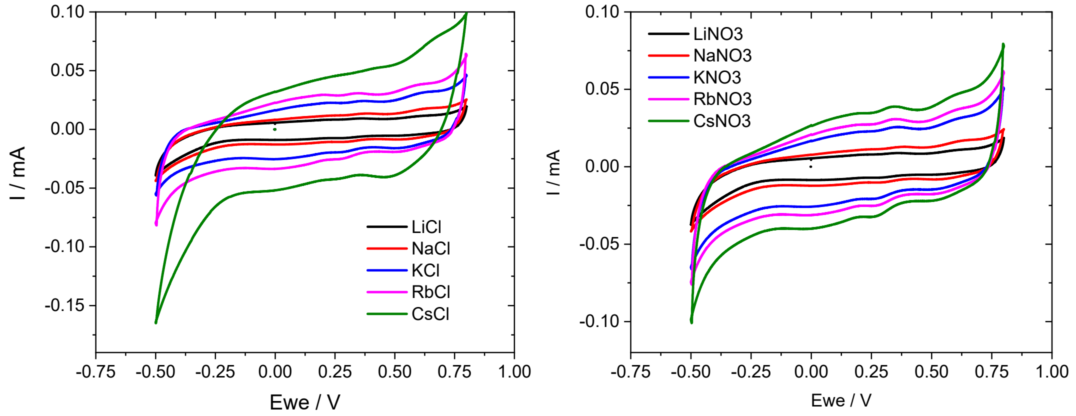

Figure S13. CV cycles in a range from -0,8 V to 0,5 V for THPP@GO in nitrates electrolytes (left) and chlorides (right).

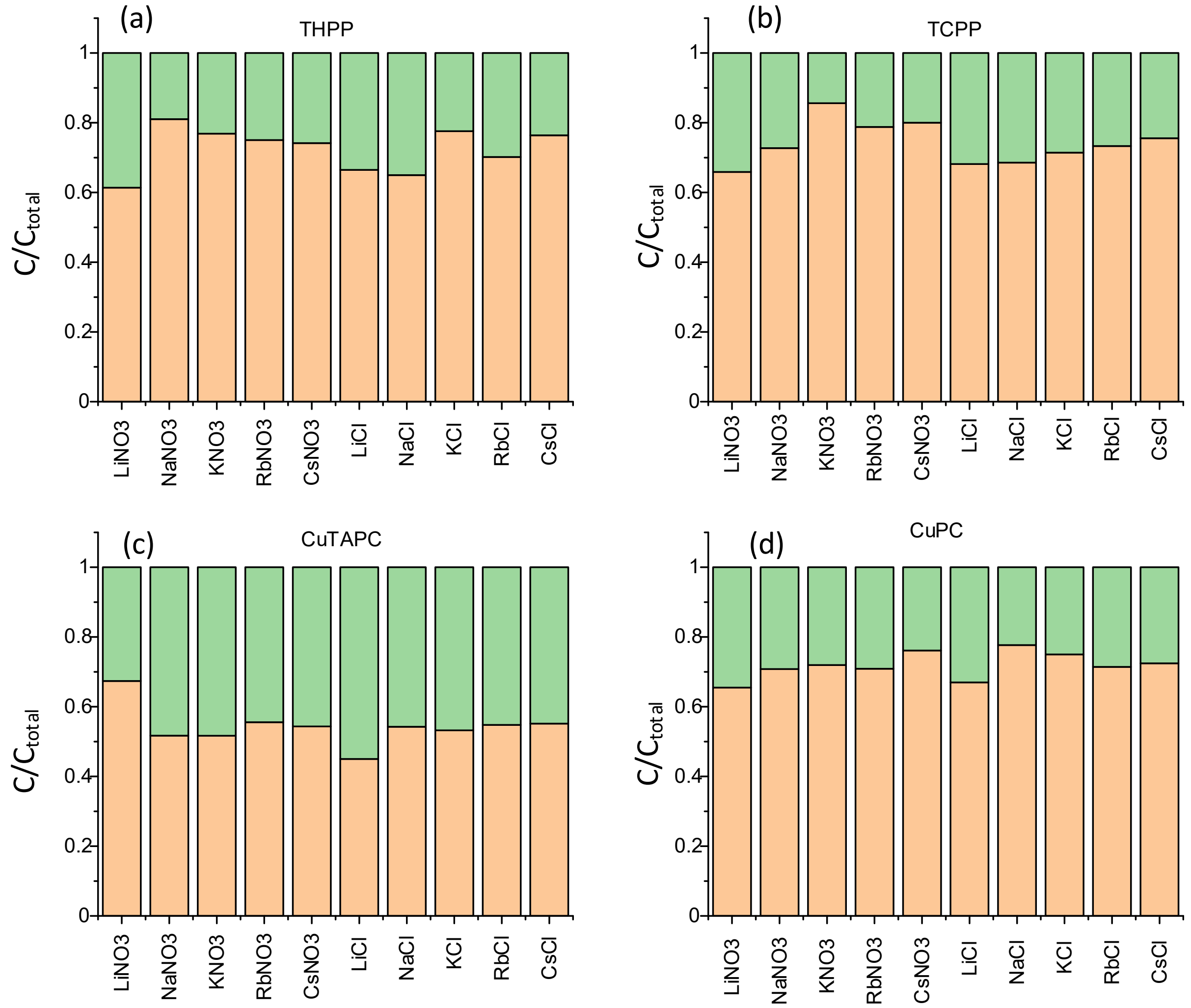

Figure S14. Contributions of Faradaic processes (green) and intercalation (orange) to the total capacitance of tetrapyrrole-modified GO electrodes in various electrolytes.

Electron Paramagnetic Resonance Spectroscopy

In the previous study, EPR spectroscopy was used to evaluate the concentration of free electrons in GO-THPP and GO-TCPP supramolecular composites. Those measurements indicated significant influence of peripheral substituents on the total electron density of the composite: in the presence of THPP threefold increase of free electron concentration was observed, whereas threefold decrease (vs neat GO) was observed in the case of TCPP.

Figure S15 presents room temperature EPR spectrum of CuTAPC and the spectra of composite CuTAPC@GO collected at 5, 100 and 300 K. EPR spectrum of CuTAPC, similarly as in the case of CuPC, consists slightly nonsymmetrical line, but described by different value of effective *g*-factor, g_{eff} = 2.0855 (± 0.0010). In the CuTAPC@GO system, in contrast to pure GO or CuPC@GO hybrid, there is a clear weakening of the EPR line from free electrons, which indicates their pairing, which can lead to a lowering of transport properties, including electrical conductivity. The line from free electrons is characterized by the value of spectroscopic coefficient g = 2.0031 (± 0.0005) and this value is very close to GO or CuPC@GO system. For the CuTAPC@GO sample, in contrast to the CuPC@GO, one can observe a significant weakness of the exchange interaction of copper ions, which allows to determine, directly from the spectrum, spin Hamiltonian parameters. EPR spectrum of CuTAPC@GO consists two axial copper complexes with the following spin Hamiltonian parameters: Cu^{2+}(1) with A_{II} = 225 (± 5) Gs, g_{II} = 2.1617(± 0.0030), $g_{\perp}$ = 2.0918 (± 0.0010), and Cu^{2+} (2); A_{II} = 140 (± 5) Gs, g_{II} = 2.3623(± 0.0030), $g_{\perp}$ = 2.0918 (± 0.0010), where A_{II} describes hyperfine interaction in parallel orientation, i.e. along the direction perpendicular to the plane of the molecule CuTAPC in CuTAPC@GO system. It should be noted that the parameters for Cu^{2+}(1) are very similar to the CuPC diluted in various solutions but the EPR parameters of Cu^{2+}(2) ion indicate formation of a completely new copper complex. A large change of spin Hamiltonian parameters in the parallel orientation $A_{II}(Cu^{2+}(2))$ and $g_{II}(Cu^{2+}(2))$ (perpendicular to the plane of the CuTAPC particle) indicates a strong interaction of the Cu^{2+} ion with GO. The ratio of free electrons: Cu^{2+} at 5 K in CuTAPC@GO amounts to 0.025:100 and is 24 times smaller than in the CuPC@GO complex (*vide infra*).

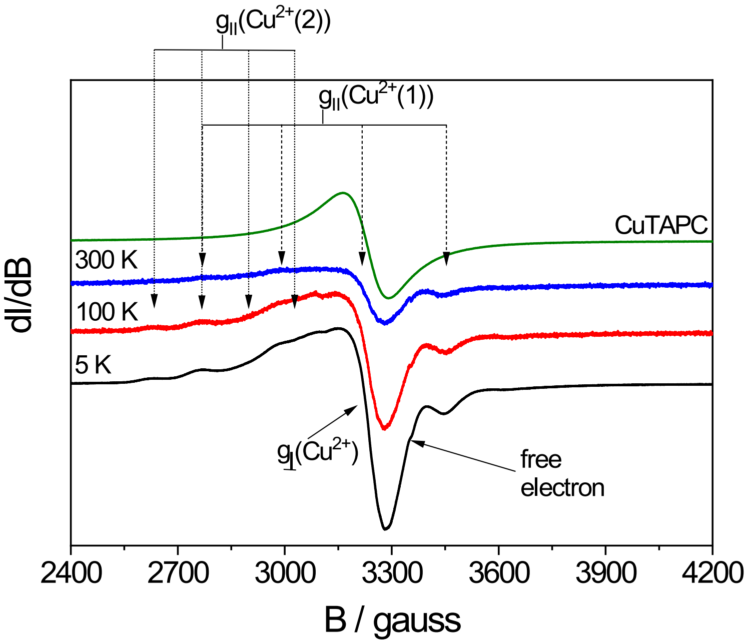

Figure S15. EPR spectra of CuTAPC (green curve, recorded at room temperature) and of the CuTAPC@GO composite recorded at 300, 100 and 5 K. Arrows indicate EPR line positions of Cu^{2+} ions and free electrons.

Figure S16 presents EPR spectrum of CuPC recorded at room temperature (RT) and spectra of composite CuPC@GO collected at 5, 100 and 300 K. An exchange interaction between Cu^{2+} ions in CuPC sample leads to an averaging of anisotropy of the g-tensor and hyperfine structure A, therefore EPR spectrum consists only slightly nonsymmetrical line characterized by effective g-factor g_{eff} = 2.0655±0.0010. For CuPC@GO composite material an effective g-factor is significantly changed: g_{eff} = 2.0613 (± 0.0010), 2.0590 (± 0.0010) and 2.0546 (± 0.0010) at 300, 100 and 5 K, respectively. The change of g-factors can be attributed to the interaction of the components. In addition to the signal from copper ions, a line with g = 2.0027±0.0005 from free electrons is visible. Moreover, the EPR spectrum of CuPC@GO consists a weak sextet assigned to traces of Mn^{2+} ions, which are a post-synthetic impurity. Due to the Cu^{2+}, Mn^{2+} and free-electron EPR line overlapping, it is difficult to quantify the number of localized, delocalized and thermally activated radicals as in our previous work. At the lowest temperature (5 K), where localized electrons dominate in the EPR spectrum, the ratio of the number of centers Cu^{2+}:Mn^{2+}:free electrons can be estimated as 100:2.7:0.6.

Increased free electron concentration is usually associated with capacitive properties and electrostatic irregularities at the surface of GO. Combined experimental and theoretical investigations attribute paramagnetic centres of GO to defect states (unsubstituted carbon atoms in highly derivatized areas) and to electrons trapped in extended aromatic regions. These defects and aromatic areas may, in turn, due to higher local charge density, be effective centres of cation binding, thus contributing to capacitive effects as shown in previous studies.[1-5] In the case of THPP and TCPP the changes in spin concentration coincide with the changes incapacitance (i.e. increased capacitance is associated with increased spin concentration and *vice versa*), thus supporting this hypothesis. The case of copper complexes cannot be that clearly explained due to more complex magnetic structure of these materials.

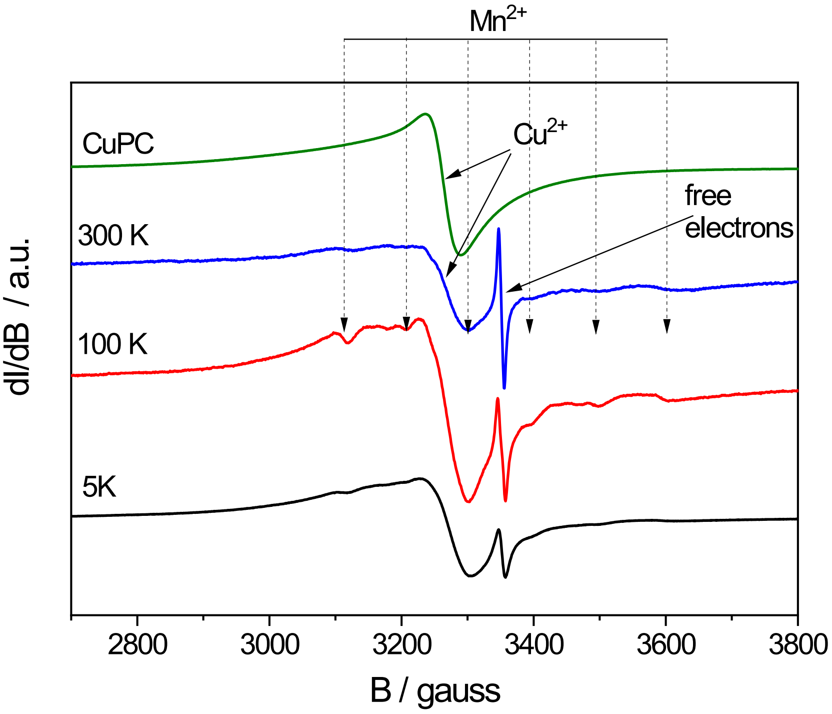

Figure S16. EPR spectra of CuPC (green line, recorded at room temperature) and the CuPC@GO supramolecular composite recorded at 300, 100 and 5 K. Arrows indicate EPR line positions of Mn^{2+}, Cu^{2+} ions and free electrons.

References

1. W. J. Lee, J. Lim and S. O. Kim, *Small Methods*, 2017, **1**, 1600014.
2. Q. Ren, N. Qin, B. Liu, Y. Yao, X. Zhao, Z. Deng, Y. Li, Y. Dong, D. Qian, B.-L. Su, W. Zhang and H.-E. Wang, *Journal of Materials Chemistry A*, 2020, DOI: 10.1039/C9TA11965E.
3. Y. Xu, C. Zhang, M. Zhou, Q. Fu, C. Zhao, M. Wu and Y. Lei, *Nat Commun*, 2018, **9**, 1720.
4. C. Ma, X. Shao and D. Cao, *Journal of Materials Chemistry*, 2012, **22**, 8911-8915.
5. L.-J. Zhou, Z. F. Hou and L.-M. Wu, *The Journal of Physical Chemistry C*, 2012, **116**, 21780-21787.